Evaluating Smartphone LiDAR for Road Infrastructure Mapping: Harmonisation of iPhone LiDAR Data with National Airborne LiDAR Datasets

Daan H. van der Heide[1,2], Tessa Eikelboom[2], Jantien E. Stoter[1]

[1] Dept. of Urbanism, Architecture Faculty, Delft University of Technology, Delft, the Netherlands

[2] Centrale Informatie Voorziening, Rijkswaterstaat, Derde Werelddreef 1, Delft, the Netherlands

daan.vander.heide@rws.nl, tessa.eikelboom@rws.nl, J.E.Stoter@tudelft.nl

Keywords: LiDAR, smartphone scanning, point clouds, infrastructure monitoring, road markings, data harmonisation

Abstract

National airborne laser-scanning campaigns, such as the Dutch AHN update, run on multi-year cycles, leaving newly built infrastructure undocumented for years. This study investigates whether smartphone LiDAR can close that gap by harmonising iPhone-acquired point clouds with the national dataset, using road markings as shared geometric reference features. A four-stage workflow is proposed: data acquisition, road-marking extraction, transformation from a local to the national reference frame, and voxel-based harmonisation, demonstrated on a simulated highway ramp at the Future Mobility Park in Rotterdam using an iPhone 17 Pro and two free acquisition packages, RDTAB (S1) and Modelar (S2). Variations in acquired data volume and preprocessing between the packages helped assess harmonisation with the national point cloud, based on the resulting points, RGB values, and spatial distribution. The case study showed registration accuracies of 0.039 m and 0.164 m against GNSS control points, with positioning error as the main factor affecting altimetric accuracy, which ranged from 0.053 to 0.170 m. The average ICP cloud-to-cloud difference across both packages and the national point clouds was 0.032 m. These results indicate that smartphone LiDAR is accurate and low-cost enough to serve as a complementary, not alternative, data source for high-frequency updates between national mapping campaigns.

1. Introduction

In recent years, the LiDAR sensor integrated into the iPhone Pro lineup has gained increasing attention. Originally developed for film and augmented-reality applications, this technology is now being explored for geographic and geospatial purposes. Compared with professional instruments such as terrestrial laser scanners or mobile laser-scanning systems, smartphone LiDAR sensors are significantly cheaper and easier to deploy. Previous studies have shown that these sensors can produce usable three-dimensional point clouds with minimal preparation, enabling rapid out-of-the-box data acquisition.

Although smartphone LiDAR sensors generally provide lower spatial accuracy than professional systems, their rapid deployment offers advantages for infrastructure monitoring. In many situations, infrastructure elements are modified or added between scheduled national acquisition campaigns. When such changes occur, rapid updates to existing three-dimensional datasets may be required. Smartphone LiDAR sensors provide a practical solution in these scenarios because they can be deployed quickly without specialised equipment. A brief on-site scan is sufficient to update an existing digital representation of the environment.

National and regional airborne LiDAR acquisition campaigns typically operate on multi-year update cycles. Consequently, newly constructed infrastructure may remain undocumented for extended periods. Smartphone LiDAR sensors could therefore act as complementary data sources for capturing high-frequency updates between official acquisition campaigns. However, despite the increasing availability of smartphone LiDAR technology, limited research has examined its applicability in road infrastructure environments, such as highways and tunnels.

This research investigates whether smartphone LiDAR data can be harmonised with large-scale point-cloud acquisition frameworks. In particular, the study explores the use of road markings as geometric reference points to align locally acquired smartphone scans with national airborne LiDAR datasets. The proposed workflow aims to address temporal gaps in national acquisition campaigns while maintaining compatibility with existing geospatial datasets.

The main technical contribution of this study is to demonstrate the effects of out-of-the-box, low-cost LiDAR sensors, using road markings as benchmarks for point cloud alignment in the harmonisation process. In infrastructure monitoring, a smartphone-based handheld scanner could serve as an alternative for providing low-resolution updates to the national dataset for temporal change studies. This study, therefore, attempts, in a small case-study setup, to validate the sensor's effectiveness by using only the iPhone as the main sensor, compared to the traditional GNSS measurement strategy. The study is further limited to using only open-source software that is free of charge to the user at the time of writing, to keep the system as low-cost as possible.

2. Related work

2.1 Smartphone LiDAR accuracy

Scientific studies evaluating smartphone LiDAR sensors began shortly after the release of the iPhone 12 Pro in 2020. These early studies primarily focused on assessing the accuracy and usability of smartphone-based scanning systems. The laser is emitted at the near infrared spectrum in a 2D array from a Vertical Cavity Surface Emitting Laser (VCSEL) (MacKinnon, 2018, Luetzenburg et al., 2021). Hardware improvements have since been introduced across device generations. For example, the iPhone 12 Pro incorporated the Sony IMX590 LiDAR sensor, while newer devices such as the iPhone 15 to 17 Pro use the updated Sony IMX591 sensor (Yole SystemPlus, 2023), aiming to maintain equivalent spatial precision while improving power efficiency and sensor performance.

Several studies have evaluated the accuracy of smartphone LiDAR sensors across different environments. In forestry applications, diameter-at-breast-height estimation has achieved accuracies below 0.001 m RMSE when point densities exceed approximately 600 to 700 points per square metre (Korznikov et al., 2026, Výbošťok et al., 2025).

Image-based reconstruction combined with LiDAR measurements has also achieved high accuracy when image overlap exceeds 95% and ground sampling distances remain below 5 cm. Laboratory experiments have reported mean absolute errors of approximately 0.53 cm and RMSE values of approximately 0.63 cm at capture distances below 5 m (Výbošťok et al., 2025).

Field studies using iPad Pro LiDAR scanners have reported RMSE values of around 1.5 cm in forest environments with varying vegetation densities (Výbošťok et al., 2025). More recent studies using smartphone LiDAR sensors report RMSE values ranging from approximately 1.6 cm to 5.3 cm, depending on environmental conditions (Khan and Kumar, 2026, Bondar et al., 2026). The studies by (Tavani et al., 2022, Korznikov et al., 2026) suggested that smartphone LiDAR sensors can achieve sub-centimetre accuracy under controlled conditions. In contrast, in real-world environments, RMSE values typically range from approximately 1 cm to 3 cm.

Most existing research focuses on relatively small-scale environments such as building interiors or geological outcrops. Another frequently discussed topic in the literature is the cost-benefit ratio of smartphone LiDAR systems. The study of (Khan and Kumar, 2026) even suggested that smartphone scanning can be up to 25 times cheaper than professional scanners. Given this cost advantage, smartphone LiDAR sensors present a comparatively inexpensive alternative for point cloud acquisition, though their viability at infrastructure scale has yet to be demonstrated.

2.2 Road-marking extraction from point clouds

Road marking extraction is a well-studied benchmark task, in part because it underpins self-driving vehicles that rely on either LiDAR or camera data (Yang et al., 2020). Markings are typically detected either by their distinctive white colour or by an intensity spike relative to the surrounding concrete, combined with their rectangular shape (Chen et al., 2023, Soilán et al., 2022). Techniques for road marker extraction have also been applied to mobile laser scanning (Pan et al., 2019), using image reconstruction to detect markings and match them to their corresponding classes from a vehicle's perspective.

Capture approaches differ: some studies extract markings directly from variable intensity values (Guan et al., 2014, Kumar et al., 2014). In contrast, others reconstruct multi-symbol shapes using machine learning algorithms trained on an embedded database, applying density-based point grouping to determine the correct geometric shape of each marking (Bailo et al., 2017). The technical challenge for this study, however, lies not in the extraction algorithms themselves but in applying these models to a point cloud captured on a smartphone. Most existing models target a broader scope than intended here; a simple image-filtering step, on which many of them rely, was deemed sufficient to produce a binary image of the road markings for applying common image segmentation techniques (e.g., Canny edge detection).

The two acquisition methods this study aims to harmonise, Airborne Laser Scanning (ALS) and handheld scanners, also differ in how road markings can be extracted. ALS acquires points at a lower density and wider spacing than the handheld scanner, with the exact spacing depending on acquisition angle, altitude, and sensor overlap. As a result, markings on smaller-scale infrastructure can be missed. The handheld scanner offsets this with denser, closer-range coverage, but at the cost of the broader environmental context that ALS captures from altitude

2.3 Point-cloud registration and harmonisation

There are three approaches to point-cloud registration, one of which involves harmonisation between point clouds. The first are coarse alignment methods. Where the point cloud datasets are closely aligned iteratively, so that the points line up. Then, a more refined approach, such as the ICP methodology, is used. These steps are required to register each point cloud relative to the other and determine the error between the two datasets measured at different temporal moments. Examples include using real-life features such as house ridges or road markings, which are now relatively stable over time (Lindenbergh and Pietrzyk, 2015, Huang et al., 2022, Stilla and Xu, 2023).

Aligning and harmonising point clouds from different sources is non-trivial: (Huang et al., 2022) outline the trade-offs involved and the criteria needed to decide, for each point or feature, whether conflicting data should be rejected or fused. Two extremes illustrate the problem: replacing the entire scene with the new dataset discards everything from earlier captures, while keeping the geometry as an exact copy of the previous dataset and updating only its attributes hides which source actually determined the outcome. A voting-based system avoids both pitfalls by resolving conflicts on a per-point basis using evidence from all contributing datasets, while maintaining an auditable record of which dataset drove each decision.

2.4 National airborne LiDAR programmes

Among European countries, national airborne laser-scanning point clouds are commonly regarded as the primary elevation dataset. In the Netherlands, that is the Actueel Hoogtebestand Nederland, which is acquired over 3 years. The sixth iteration has recently started, which includes RGB values. When RGB values for the AHN are needed to compare different versions of the AHN and to highlight temporal differences between national acquisition campaigns, the Geotiles (van Natijne and TU Delft Optical and Laser Remote Sensing Group, 2023) project provides a method for adding national program imagery to the point data.

The specifications for AHN4 and AHN5 point cloud datasets are given in Table 1 (Het Actueel Hoogtebestand Nederland, 2024). The accuracy in the table consists of the planimetric [m] and altimetric [m] accuracies, while the spatial distribution is the minimum requirement specified in the specifications

Name	Acquisition year	XY;Z Accuracy [cm]	Spatial distribution [ppsm]
AHN4	2020	13; 10	10 to 14
AHN5	2023	13; 10	10 to 14

Table 1. Specifications of the AHN airborne LiDAR dataset (accuracy and spatial distribution) at the case-study area.

3. Methodology and data

3.1 Overall workflow

To investigate the integration of smartphone LiDAR data with national mapping datasets, this study proposes a workflow consisting of four processing stages: (1) data acquisition, (2) road-marking extraction, (3) transformation from a local reference frame to a national coordinate system, and (4) point-cloud alignment and harmonisation with the national dataset. The overall workflow is illustrated in Figure 1, which summarises the proposed integration procedure.

As the goal is to achieve an aligned and harmonised point cloud, the one with higher temporal resolution is selected. Here, temporal resolution refers to the recency of a point cloud's acquisition date, used as a proxy for how likely it is to reflect the infrastructure's current state, distinct from the multi-year update cycle between AHN campaigns (Section 1) or the acquisition frequency a smartphone workflow could support (Section 5). Both point clouds are voxelised on the same grid so that each voxel can be evaluated independently. For every voxel populated by both datasets, the acquisition dates of each dataset are compared, taken per point where available, or, otherwise, as the dataset-level survey date, and only the points from the more recently acquired dataset are retained for that voxel, with the other dataset's points discarded. Voxels populated by only one dataset are left unchanged, since there is no competing data to arbitrate.

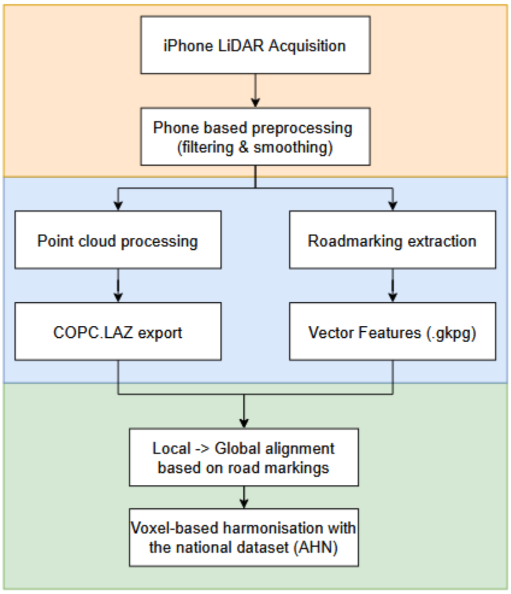

Figure 1. Workflow method for smartphone LiDAR harmonisation.

3.2 Data acquisition

For this study, the iPhone 17 Pro is used, with two different software packages to create redundancy and validate the software's error-smoothing algorithms. Both software packages rely on position estimation on the imu and set the 0,0,0 coordinate at the start of the acquisition. Table 2 shows the different software packages, including the version used, while also defining the acronym used in the article.

Software package	Version	Study unique ID
RDTAB	0.22.0	S1
Modelar	3.0.0	S2

Table 2. Overview of the acquisition software packages used in this study.

To increase the efficiency of the harmonisation method, the point clouds from both software packages were converted from the e57 format to a cloud-optimised data format (COPC.LAZ) to optimise spatial indexing and streaming, rather than loading the full 1.97 GB in memory. The study used the LAZ-to-COPC conversion in QGIS 4.0.1 to generate the COPC files for the processing pipeline.

The data are captured in a push-broom pattern, in which each lane is walked up and down to ensure sufficient overlap. While the weather conditions were favourable and sunny, RGB values were captured on a dry surface. The measurement was conducted at a normal walking speed (3 km/h), with the scanner positioned between 0.8m and 1.3m above the ground.

Each software package recorded repeated passes along the ramp, allowing the positioning error to be compared between independent runs of the same route. S1 acquired 0.142 GB of combined point cloud data, including RGB data. While using the S2 package, a total of 1.9 GB was acquired, including the RGB dataset; this difference in file size reflects each package's own point-thinning and metadata overhead rather than a difference in scan coverage.

3.3 Case-study environments

To evaluate the feasibility of smartphone LiDAR scanning for infrastructure monitoring, two case-study environments were selected. Since measurements on active highways are difficult without road closures, a controlled simulation environment was created at the Future Mobility Park in Rotterdam. This environment replicates highway infrastructure conditions while enabling safe, repeatable data-acquisition experiments. In Figure 2, the orange dots represent the GNSS control points used for the local-to-global datum transformation. Please note that the lines represent the cross-profiles of Figure 6 and 7 respectively.

Figure 2. GNSS points for the local-to-global datum transformation, pictured on drone shots taken during the case study, including the cross-profile lines of Figure 6 and 7.

The reference data for this case study was AHN5, as this is the last dataset available for this region from the national dataset. The road markings were constructed in accordance with Dutch road standards, with a fixed 3 m length and a 9 m interval, using dashed lines 0.15 m wide, while the solid lines are 45 m long and 0.15 m wide.

3.4 Road-marking extraction

The road-marking extraction will be key to transforming the locally acquired, low-cost smartphone sensor into the national dataset. The extraction consists of different steps based on the RGB values. Since the smartphone data lacks intensity values, the automated extraction should not rely on intensity-based scattering.

The local datasets are projected onto a 2D RGB raster with a resolution of 0.02 m. Such that white pixels can be extracted and, using Canny edge detection, boundaries can be drawn. From the polygons, the corners are extracted from the datasets using the Douglas-Peucker method (Source). As strict error validation is required, the following logic applies: a marking can have only one centroid and four corner points. As such, the dashed line shows the constructed pattern, while the solid line is filtered based on the RGB values and the best-fitting rectangle.

Since the lines follow a pattern, the centroids are used as a quality check for automated benchmarking. The road markings in the Netherlands are constructed on highways in a very specific pattern, which, in the case study environment, is a dashed pattern of a 3m stripe with a 9m gap between 2 solid marking lines perpendicular to each other. Hence, the extraction algorithm validates the pattern to determine whether any markings were missed or to reject falsely detected markings in the point cloud dataset. An example of S2 is given in Figure 3, where the green markings are the accepted markings after the extraction process, and the red markings are the rejected/false markings.

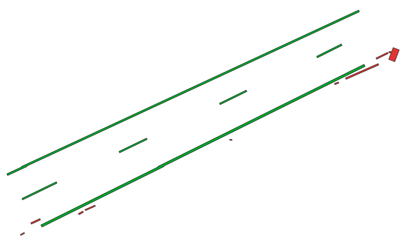

Figure 3. Effects on the roadmarking extraction of S2, where red indicates the rejected markings and green the accepted markings.

The resulting road markings are shown in Figure 4 and compared with the actual markings, with purple indicating the S1 and green the S2 data plotted over the captured drone images of the case study area.

As these markings are newly constructed, the AHN reference dataset does not yet contain them. The smartphone-derived road-marking corner points are therefore registered directly to the GNSS control points, which carry the national datum, rather than to markings in the AHN itself, with the GNSS position taken as the true value. As no independent accuracy estimate exists for this substitution, it is assumed to have the same standard error as the AHN's own accuracy relative to the national control points, which is 10 cm (Het Actueel Hoogtebestand Nederland, 2024).

Before extraction, the raw smartphone point clouds are filtered to remove any outliers and isolated noise using a statistical or

Figure 4. Extracted road-marking corner points (purple: S1; green: S2) overlaid on drone imagery of the case-study area.

radius-based outlier filter. The road surface is then separated from the elevation data for the ground-segmentation step using a locally fitted plane. As the local data is a more focused and flexible scan, the vegetation and objects in the case-study area were not surveyed. The road segmentation preprocessing step restricts the subsequent RGB raster to the drivable surface, reducing false detections from markings outside the carriageway, walls, and roadside vegetation.

3.5 Local-to-national datum transformation

The smartphone laser sensor, in combination with the open software packages, measures the point cloud in a local system. Hence, a translation is required between the local dataset and the national georeferenced dataset. In this study, we used a matching workflow to iteratively find the best match between the road markings' corner points and the GNSS points. RANSAC is used for the coarse coordinate transformation. When the points lie within a certain threshold, the ICP is used for the finer alignment. The transformation parameters between the local and national datasets are used to transform coordinates from the local to the national dataset.

3.6 Voxel-based harmonisation

To conduct the final step, it is assumed that, with the local-to-national datum transformation, the road markings serve as benchmarks. The assumption, therefore, is that both point clouds overlap within a certain spatial range. Therefore, a grid can be constructed that represents both the national and local point clouds. Then the voxel grid can be created with a fixed interval; this study chose a 0.025 m $\times$ 0.025 m interval to ensure that road markings are captured across multiple voxels, with points representing the concrete to determine the variation in the road.

In each voxel, a decision is made based on the points present and on a comparison between the national and local datasets. The harmonisation process is designed to reject the lowest-scoring point cloud for the voxel. The criteria used to compare a cloud are weighted by the user. Each situation requires a tailored approach to harmonising the local and national datasets. This study has set 4 main criteria, which can influence the alignment:

1. Temporal resolution
2. Spatial variation between RGB values and distribution
3. Overall spatial resolution of the dataset
4. Metadata (e.g., presence of classification, etc.)

For the first criterion, the point cloud with the more recent acquisition date (Table 1) is scored as the winner: for example, between a point cloud acquired in 2025 and one acquired in 2026, the 2026 dataset takes precedence for that voxel. For the second criterion, the point cloud containing RGB information is selected as the winner: a dataset with RGB values is assigned a score of 1, and one without is assigned a score of 0. For the third criterion, the point cloud with the finer spatial resolution, i.e., the smaller point spacing or higher absolute accuracy, is scored as the winner. For example, between a point cloud with a 1 mm point spacing and one with a 1 cm point spacing, the 1 mm dataset takes precedence for that voxel. For the fourth criterion, the point cloud with the most available metadata (e.g., classification, intensity, return number) is selected as the winner.

Each criterion, therefore, yields a binary score $s_c \in \{0, 1\}$ per point cloud, where $s_c = 1$ indicates that the point cloud wins that criterion for the voxel under consideration. The four per-criterion scores are combined into a single weighted score,

$$S = w_1 s_1 + w_2 s_2 + w_3 s_3 + w_4 s_4, \tag{1}$$

where $w_1, \ldots, w_4$ are user-defined weights reflecting the relative importance of each criterion, subject to $\sum_{c=1}^{4} w_c = 1$. For each voxel, the point cloud with the higher combined score S is retained, and the other is rejected. In this study, temporal resolution was weighted twice as heavily as each of the remaining three criteria, as the aim was to test smartphone data as a complement to national point cloud acquisition campaigns.

The final step, based on voxel harmonisation, is to align the local data specification with the national datasets. The same spatial distribution is used as for the national dataset, while retaining all metadata from both point clouds. An additional metadata field is introduced to highlight the harmonisation between the two datasets. The data is exported as a point cloud (COPC.LAZ) and a digital terrain model at a 0.5 m grid size.

3.7 Evaluation criteria

To evaluate the smartphone sensor, the relative accuracy of its point cloud is assessed. Positioning errors caused by drift in the z-axis form the first evaluation criterion: the point cloud is compared against a fictitious plane fitted through the road-marking corner points, assuming a relatively flat road surface, to determine the altimetric residuals introduced by the acquisition. The residuals of the road-marking transformation applied to GNSS points serve as a second criterion, since road markings are considered an ideal benchmark for road infrastructure due to their high visibility in RGB point cloud datasets.

4. Results

4.1 Acquisition and point density

The RGB attributes of the smartphone scans differ from those recorded in the airborne LiDAR dataset. Still, the smartphone scans exhibited substantially higher point densities than the AHN dataset, which typically contains approximately 10 points per square metre (ppsm). The statistical results are presented in Table 3, where each software package's resulting point cloud is accompanied by its corresponding density values. Please note that the mean density is determined per 2D grid, e.g. higher densities in urban areas due to mutiple points per XY.

4.2 Relative altimetric accuracy

To validate altimetric accuracy using smartphone dataset error metrics and assess data consistency, variations were computed between the point cloud and a fictitious linear plane passing through the road's corner points. The variation between the plane and the point cloud is given in Figure 5, with a range for S1 between -0.4m and 0.4m and for S2 between -0.3m and 0.3m.

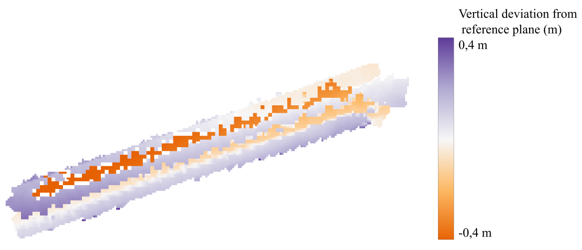

(a) Vertical variation of S1 between the point cloud and the fictitious linear plane.

(b) Vertical variation of S2 between the point cloud and the fictitious linear plane.

Figure 5. Deviation between the smartphone point clouds and a fictitious linear reference plane through the road corner points (a) S1; (b) S2.

A clear artefact of the surveyor's walking pattern is visible at the end, at 0.4m for S1 and 0.3 m for S2: the positioning error becomes apparent along the walking path, with no coherence between data points across passes. In the northern part of the Smartphone point cloud, the error increases more sharply, coinciding with where the winding pattern begins and ends; as a result, on longer trajectories, the error drifts further, and the smartphone data eventually becomes unusable.

To highlight the variations between the datasets, the following cross-profiles are provided in Figure 6 and 7. The top figure shows the cross-sections of S1, while the bottom shows the results for S2. In Figure 2, the cross-profiles given are indicated with letter labels. In total, the error observed in the fictitious linear plane drawn through the case study area can be attributed to the classification of the ground class, with a 5 cm error between the different datasets. The drift is most pronounced in the lower-lying parts (A' to A") of the dataset, where the point clouds are less well vertically aligned with one another, a consequence of the inertial measurement unit (IMU) failing to compensate for altimetric drift while walking the proposed pattern.

Software package	Points acquired	Mean 2D density [ppsm]	Average point spacing [m]
S1	5,603,681	11916.4	0.009
S2	512,610,364	1124145.5	0.010
AHN4	42,012	92.1	0.104
AHN5	16,672	36.6	0.165

Table 3. Acquisition statistics per software package compared with the AHN national dataset.

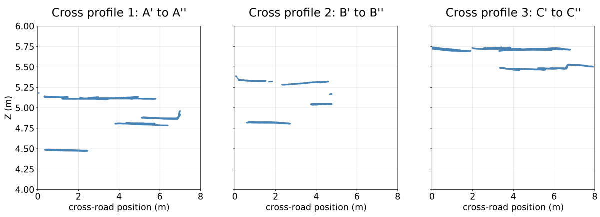

Figure 6. Cross-profiles of the S1 software point cloud depicted from the labeled points in Figure 2, with a vertical range between 4m and 6m

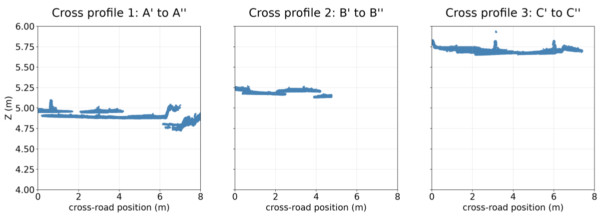

Figure 7. Cross-profiles of the S2 point cloud depicted from the labelled points in Figure 2, with a vertical range between 4m and 6m.

Based on both software acquisitions, the errors observed in the cross profiles are caused by repeated passes not being automatically referenced to one another and by incidental movement of the handheld scanner independent of the walking path. Independent scans of the same route can differ by approximately +/- 0.4m in the vertical direction. Neither software package compensates for this during acquisition, and the discrepancy only became apparent during post-processing, once the scans had already been collected.

4.3 Road-marking extraction, registration and harmonisation accuracy

Figure 4 of Section 3 shows the extracted road-marking data from the S1 (purple) and S2 (green) smartphone point clouds overlaid on the drone-captured image of the case study area. The resulting overview of the harmonised point clouds, based on this road-marking alignment, is given in Figure 8, where (a) and (b) provide the S1 data with AHN4 and AHN5, and (c) and (d) provide the S2 point cloud harmonised with the national datasets. Here, the harmonisation of point density and RGB values was set to the average relative to the national dataset.

The results are presented in Table 4, which shows the transformation residuals, the relative altimetric accuracy of the smartphone point cloud, and the ICP cloud-to-cloud variation between the different versions of the AHN and the smartphone data from the two software packages.

The results showed that smartphone data can be used as a complement to between-temporal changes in infrastructure for objects with minor z-variations, with a total average cloud-to-cloud difference of 0.032 m across both national datasets and software packages.

5. Discussion

This study has four main limitations that affect the smartphone's applicability, given the scope and the case study area of the research. First, it evaluates a single device generation, the iPhone 17 Pro, so the results cannot yet be generalised to earlier or future sensor hardware. Second, the case study was conducted in a controlled environment at the Future Mobility Park rather than on an operational highway, where traffic, variable lighting, and time pressure would likely degrade both the acquisition quality and the walking pattern assumed in the workflow. Third, the reliance on RGB for the smartphone data and calibrated intensity for the AHN data means the two extraction pipelines are not fully equivalent, and any systematic difference between them is difficult to separate from genuine registration error. Fourth, the current experiments do not include tunnels, where GNSS control points are unavailable, and the workflow's dependence on a GNSS-anchored datum transformation would need to be rethought.

The ICP cloud-to-cloud differences in Table 4 remain at the centimetre level (0.004–0.062 m), within or near the 0.01–0.03 m range Section 2.1 identifies as typical for smartphone LiDAR outside laboratory conditions (Tavani et al., 2022, Korznikov et al., 2026). The roadmarking transformation residuals are more mixed: S1 - 0.039 m sits close to this range, but S2 - 0.164 m falls clearly outside it. This places cloud-to-cloud performance broadly in line with forestry and geological applications, rather than the sub-centimetre results of (Výboštok et al., 2025) obtained under controlled, short-range laboratory conditions. However, the S2 registration result shows that this comparison does not hold uniformly. For high-frequency interim updates between national point cloud acquisition campaigns, an accuracy of this order is sufficient to detect the presence and gross geometry of new infrastructure, such as newly painted road markings.

One of the main discussion points is the low resolution of the smartphone GNSS sensor. As both software packages rely heavily on the imu sensor and positioning method, the z-axis drift becomes noticeable in the case study. As this study assumes that users of the low-cost smartphone want to use no additional sensors out of the box or pay for a software subscription, the reported accuracy should be read as relative rather than absolute. Professional users in the literature show higher values when using the traditional benchmarks for overlapping datasets. The relative accuracy would have been higher with an additional GNSS sensor, combined with the phone's IMU. Three mitigation strategies could extend this limit: periodic re-anchoring to GNSS control points along the route rather than only at the start and end; closing the loop by returning to the first control point, which distributes the accumulated drift back across the trajectory.

The voxel-based harmonisation process is a simple application method, but it is not flexible enough on a point level. The study acknowledges that the shapes and context are important for determining whether a voxel should be rejected or retained in a

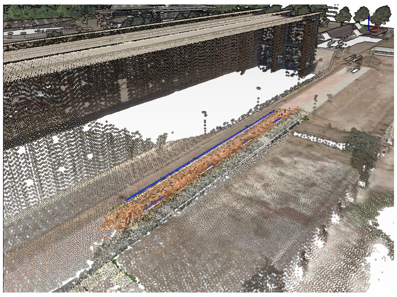

(a) S1 point cloud harmonised with AHN4

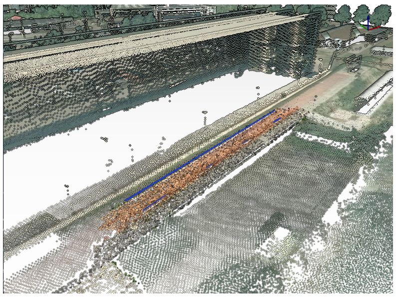

(b) S1 point cloud harmonised with AHN5

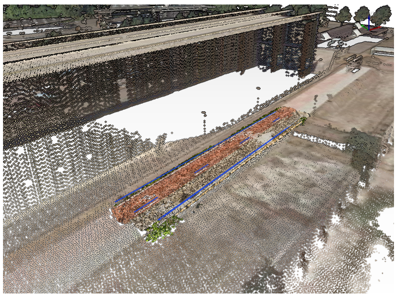

(c) S2 point cloud harmonised with AHN4

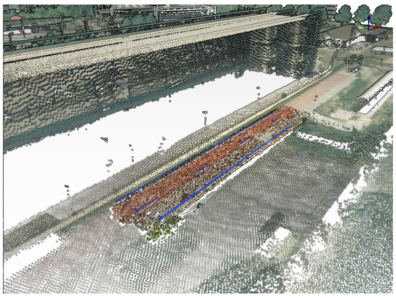

(d) S2 point cloud harmonised with AHN5

Figure 8. Overview of harmonised point clouds per software package and AHN reference dataset, where blue polygons illustrate the extracted markings.

Transformation stage	Relative accuracy of local data [m]	Roadmarking transformation [m]	ICP cloud to cloud average difference [m]
AHN4 vs S1	0.170	0.039	0.033
AHN5 vs S1	0.170	0.039	0.062
AHN4 vs S2	0.053	0.164	0.004
AHN5 vs S2	0.053	0.164	0.030

Table 4. Registration residuals per transformation stage: the relative accuracy of the local data and the fictual plane, roadmarking transformation to the GNSS points and the ICP cloud-to-cloud average difference in the case study area.

point cloud. In our case, there are no objects present that could have this issue, but situations where a gantry is partly rejected could occur when favouring the temporal aspect and introducing false errors. This aligns with the cases made in (Stilla and Xu, 2023), as the decision-making process in our study is too rigid to account for difficult shape differences.

The matching algorithm applied in our study is based on an iterative process. It assumes that the extracted road-marking corner points represent stable, unambiguous features that can be reliably matched between the smartphone and AHN datasets. This assumption holds reasonably well in the case-study environment, where markings are freshly painted, high-contrast, and undamaged. Still, it is less secure on operational highways, where markings wear unevenly, are often repainted slightly offset from their previous position, and can be partially obscured by traffic during acquisition.

The main advantage of road markings over artificial targets is availability. These features already exist at the required density along nearly every stretch of highway in Europe and the Netherlands, whereas placing surveyed targets would reintroduce the cost and lead time this study aims to avoid. Existing infrastructure geometry, such as gantry footings or barrier joints, could serve as a complementary reference when markings are absent or worn. However, the fact that smartphone LiDAR sensors do not export information such as pulse intensity can make feature classification more difficult than the contrast between the white paint and the grey concrete.

For national road agencies, the main operational advantage is deployment speed: a single surveyor can scan a site in minutes without the road closures, traffic management, or specialist crews that mobile mapping systems typically require. This makes smartphone LiDAR suited to interim updates, flagging that a section of infrastructure has changed and giving a rough sense of its new geometry, rather than replacing the centimetre-level accuracy of national datasets.

6. Conclusions and future work

This study set out to determine whether smartphone LiDAR can be harmonised with a national airborne dataset closely enough to serve as an interim data source between successive AHN acquisition campaigns. To answer this, a four-stage workflow, acquisition, road-marking extraction, datum transformation, and voxel-based harmonisation, was developed and applied to an iPhone 17 Pro scan of a simulated highway ramp at the Future Mobility Park, using road markings as the geometric link between the local scan and the national AHN reference frame.

The key finding is that a smartphone-derived point cloud, once aligned to the AHN dataset by road markings, registers against the GNSS control points to within 0.039 m (S1) and 0.164

m (S2), and reproduces the AHN's own geometry to within 0.004–0.062 m cloud-to-cloud across the four transformation stages tested (Table 4). Whether this can meaningfully enrich the national dataset depends on the application: it requires weighing the temporal gap between AHN campaigns against the altimetric drift documented in this study, either the per-metre drift rate seen in the cross-profiles (Figure 6 and 7) or the 0.30 to 0.4 m per-loop Figure 5. Since the road-marking corners can be extracted from the smartphone's native RGB output alone, without calibrated intensity, the full workflow can run end-to-end using only data the sensor already provides out of the box.

Thus, the smartphone's low cost and out-of-the-box deployment can be considered as a complementary point cloud between national airborne LiDAR acquisition campaigns, provided its output is treated as a relative, indicative update rather than a survey-grade replacement for the national dataset.

Future work will focus on acquiring data between interval datasets in tunnels, gantry monitoring and on infrastructure assets where ALS or mobile laser scanning data acquisition is more challenging. While aiming to deploy these sensors in real-world infrastructure environments and improving the flexibility of the voxel-based harmonisation process across cross-border regions.

Acknowledgements

This study would like to acknowledge Rijkswaterstaat for funding this research and the Future Mobility Park for constructing the small highway road markings used in the case study.

References

Bailo, O., Lee, S., Rameau, F., Yoon, J. S., Kweon, I. S., 2017. Robust road marking detection and recognition using density-based grouping and machine learning techniques. *2017 IEEE Winter Conference on Applications of Computer Vision (WACV)*, 760–768.

Bondar, D., Basova, Y., Vodka, O., Machado, J., 2026. Mobile-focused spatial inspection of industrial parts using 2D image processing and LiDAR. *Measurement*, 120522. doi.org/10.1016/j.measurement.2026.120522.

Chen, S., Wang, J., Pan, W., Gao, S., Wang, M., Lu, X., 2023. Towards uniform point distribution in feature-preserving point cloud filtering. *Computational Visual Media*, 9, 249-263. doi.org/10.1007/s41095-022-0278-4.

Guan, H., Li, J., Yu, Y., Wang, C., Chapman, M., Yang, B., 2014. Using mobile laser scanning data for automated extraction of road markings. *ISPRS Journal of Photogrammetry and Remote Sensing*, 87, 93-107. doi.org/10.1016/j.isprsjprs.2013.11.005.

Het Actueel Hoogtebestand Nederland, 2024. Kwaliteitsbeschrijving – AHN. `www.ahn.nl/kwaliteitsbeschrijving`.

Huang, R., Xu, Y., Hoegner, L., Stilla, U., 2022. Semantics-aided 3D change detection on construction sites using UAV-based photogrammetric point clouds. *Automation in Construction*, 134. doi.org/10.1016/j.autcon.2021.104057.

Khan, N. H. R., Kumar, S. V., 2026. Use of Apple iPhone LiDAR for geometric measurement of road potholes using polynomial regression based stack profile method. *Innovative Infrastructure Solutions*, 11, 93. doi.org/10.1007/s41062-025-02481-1.

Korznikov, K., Doležal, J., Fibich, P., Lanta, V., Bažant, V., Aquino-Ramírez, M., Collins-Key, S., Villanueva-Diaz, J., Altman, J., 2026. Fast and reliable: Evaluating smartphone lidar app for stem diameter measurement and tree mapping.

Kumar, P., McElhinney, C. P., Lewis, P., McCarthy, T., 2014. Automated road markings extraction from mobile laser scanning data. *International Journal of Applied Earth Observation and Geoinformation*, 32, 125-137. doi.org/10.1016/j.jag.2014.03.023.

Lindenbergh, R., Pietrzyk, P., 2015. Change detection and deformation analysis using static and mobile laser scanning. *Applied Geomatics*, 7, 65-74. doi.org/10.1007/s12518-014-0151-y.

Luetzenburg, G., Kroon, A., Bjørk, A. A., 2021. Evaluation of the Apple iPhone 12 Pro LiDAR for an application in geosciences. *Scientific reports*, 11(1), 22221. doi.org/10.1038/s41598-021-01763-9.

MacKinnon, N., 2018. Image sensor with optical communication capabilities. US Patent US 2018/0367767 A1.

Pan, Y., Yang, B., Li, S., Yang, H., Dong, Z., Yang, X., 2019. Automatic road markings extraction, classification and vectorization from mobile laser scanning data. *Int. Arch. Photogramm. Remote Sens. Spatial Inf. Sci.*, 42, 1089–1096. doi.org/10.1016/j.jag.2014.03.023.

Soilán, M., González-Aguilera, D., del Campo-Sánchez, A., Hernández-López, D., Pozo, S. D., 2022. Road marking degradation analysis using 3D point cloud data acquired with a low-cost Mobile Mapping System. *Automation in Construction*, 141. doi.org/10.1016/j.autcon.2022.104446.

Stilla, U., Xu, Y., 2023. Change detection of urban objects using 3D point clouds: A review. *ISPRS Journal of Photogrammetry and Remote Sensing*, 197, 228–255.

Tavani, S., Billi, A., Corradetti, A., Mercuri, M., Bosman, A., Cuffaro, M., Seers, T., Carminati, E., 2022. Smartphone assisted fieldwork: Towards the digital transition of geoscience fieldwork using LiDAR-equipped iPhones. *Earth-Science Reviews*, 227. doi.org/10.1016/j.earscirev.2022.103969.

van Natijne, A., TU Delft Optical and Laser Remote Sensing Group, 2023. GeoTiles: Tiled and colored AHN LiDAR point clouds. `geotiles.citg.tudelft.nl/`.

Výbošťok, J., Chudá, J., Tomčík, D., Tomaštík, J., Kadlečík, R., Mokroš, M., 2025. A Comparative Analysis of Low-Cost Devices for High-Precision Diameter at Breast Height Estimation. *Remote Sensing*, 17. doi.org/10.3390/rs17233888.

Yang, R., Li, Q., Tan, J., Li, S., Chen, X., 2020. Accurate road marking detection from noisy point clouds acquired by low-cost mobile LiDAR systems. *ISPRS Int. J. Geo-Inf.*, 9. doi.org/10.3390/ijgi9100608.

Yole SystemPlus, 2023. iPhone 15 Pro LiDAR module – technology and cost analysis. Technical report, Yole Group. https://www.yolegroup.com/product/report/iphone-15-pro-lidar-module/.